Molecular Models of Nucleic Acid Triple Helixes. II. PNA and 2′-5′ Backbone Complexes

A. R. Srinivasan and Wilma K. Olson*

Contribution from the Department of Chemistry, Wright-Rieman Laboratories, Rutgers, The State University of New Jersey, 610 Taylor Road, Piscataway, New Jersey 08854-8087

Received August 6, 1997

Abstract: We describe nucleic acid triple-helical structures containing either amide or 2′-5′ linkages, the former backbone describing the chemistry of certain peptide nucleic acids (PNA). The methodology and the starting reference frame are the same as those described in the preceding article. Apart from evaluating the possible combinations of chain conformations that connect adjacent bases on each of the three strands, we have examined the feasibility of triplex formation when neighboring Watson−Crick+Hoogsteen hydrogen-bonded base triples are displaced by small amounts along their short and long axes. The predicted triple-helical complexes are examined in terms of relevant crystallographic, spectroscopic, and calorimetric data. The computed models clarify why PNA cannot form B-like structures and also reveal principles useful for the design of other triplex-forming DNA mimics.

Introduction

The desire to attack disease at the level of the genetic message has led to the design of synthetic ligands that bind selectively to the DNA base pairs through formation of triple-helical structures.[1] While most of these gene-targeted drugs are oligonucleotides or their close analogues, a growing number of DNA mimics have appeared. The polyamide nucleic acids (PNAs), for example, bind single- and double-helical DNA in a sequence-selective manner.[2−6] Two thymine-containing PNA chains form stable right-handed triple-helical structures with single-stranded poly(dA),[7] mimicking the classical poly(U)·poly(A)+poly(U) triplex.[8] The single-crystal structure of a PNA·DNA+PNA triplex made up of one strand of polypurine DNA and two pyrimidine-linked PNAs, PNA(CTCTTCTTC)·d(GAGAAGAAG)+PNA(CTCTTCTTC),[9] however, reveals unusual features in the synthetic complex. The structure, termed a P-helix, appears to be conformationally distinct from the classical A- and B-DNA double-helical forms, with a 16-fold helical repeat and significant displacement of bases from the helix axis. The combined changes generate a central hole within the complex much larger than the characteristic cavity observed in typical A-DNA structures. While these features do not surface in molecular mechanics calculations of the PNA·DNA+PNA triplex[10,11] based on the canonical fiber diffraction model,[12] the central hole persists in the single-crystal structure of the self-complementary PNA duplex, PNA$(CGTACG)_2$,[13] and is likely to characterize the all-PNA triplex, PNA(T_{10})·PNA(A_{10})+PNA(T_{10}), recently detected in solution.[14]

The replacement of the naturally occurring 3′-5′ phosphodiester linkage of DNA by a 2′-5′ connection similarly preserves the triple-stranded complexation of A- and T-containing oligonucleotides.[15,16] Indeed, the 2′-5′-linked T_{16}·A_{16}+T_{16} triplex and a similar triplex made up of 5′-$G(GA)_5GGGA$-2′, and two strands of 5′-$TCCC(TC)_5C$-2′ are thermally more stable than the corresponding complexes of 3′-5′-linked chains.[17,18] Some of this stability may arise from the enhanced base stacking and reduced electrostatic interactions suggested by preliminary modeling studies.[17] The modified chemical backbone displaces the bases with respect to their positions in the B-DNA helix and assuming the formation of standard T·A+T base triplets, changes the groove structure of the molecular complex.[17] Single-stranded 2′-5′-linked nucleic acids also form thermally stable hybrid triplexes with duplex RNA, but not with double-stranded DNA.[19] Computational studies, nevertheless, show that it is possible to construct a sterically feasible triple-helical hybrid made up of a 2′-5′-linked thymine strand complexed via

(1) Frank-Kamenetskii, M. D.; Mirkin, S. M. *Annu. Rev. Biochem.* **1995**, *64*, 65−95.
(2) Nielsen, P. E.; Egholm, M.; Buchardt, O. *Bioconjugate Chem.* **1994**, *5*, 3−7.
(3) Mesmaeker, A. D.; Altmann, K.; Waldner, A.; Wendeborn, S. *Curr. Opin. Struct. Biol.* **1995**, *5*, 343−355.
(4) Nielsen, P. E. *Annu. Rev. Biophys. Biomol. Struct.* **1995**, *24*, 167−183.
(5) Corey, D. R. *Trends Biotech.* **1997**, *15*, 224−229.
(6) Dueholm, K. L.; Nielsen, P. E. *New J. Chem.* **1997**, *21*, 19−31.
(7) Kim, S. K.; Nielsen, P. E.; Egholm, M.; Buchardt, O.; Berg, R. H.; Nordén, B. *J. Am. Chem. Soc.* **1993**, *115*, 6477−6481.
(8) Felsenfeld, G.; Davies, D. R.; Rich, A. *J. Am. Chem. Soc.* **1957**, *79*, 2023−2024.
(9) Betts, L.; Josey, J. A.; Veal, J. M.; Jordan, S. R. *Science* **1995**, *270*, 1838−1841.
(10) Almarsson, O.; Bruice, T. C.; Kerr, J.; Zuckermann, R. N. *Proc. Natl. Acad. Sci. U.S.A.* **1993**, *90*, 7518−7522.
(11) Almarsson, O.; Bruice, T. C. *Proc. Natl. Acad. Sci. U.S.A.* **1993**, *90*, 9542−9546.
(12) Chandrasekaran, R.; Arnott, S. In *Landolt-Börnstein Numerical Data and Functional Relationships in Science and Technology, Group VII/1b, Nucleic Acids*; Saenger, W., Ed.; Springer-Verlag: Berlin, 1989; pp 31−170.
(13) Rasmussen, H.; Kastrup, J. S.; Nielsen, J. N.; Nielsen, J. M.; Nielsen, P. E. *Nat. Struct. Biol.* **1997**, *4*, 98−101.
(14) Wittung, P.; Nielsen, P.; Nordén, B. *J. Am. Chem. Soc.* **1997**, *119*, 3189−3190.
(15) Dougherty, J. P.; Rizzo, C. J.; Breslow, R. *J. Am. Chem. Soc.* **1992**, *114*, 6254−6255.
(16) Rizzo, C. J.; Dougherty, J. P.; Breslow, R. *Tetrahedron Lett.* **1992**, *33*, 4129−4132.
(17) Jin, R.; Chapman, W. H.; Srinivasan, A. R.; Olson, W. K.; Breslow, R.; Breslauer, K. J. *Proc. Natl. Acad. Sci. U.S.A.* **1993**, *90*, 10568−10572.
(18) Breslow, R.; Sheppard, T. L. *Pure Appl. Chem.* **1996**, *68*, 2037−2041.

S0002-7863(97)02721-2 CCC: $15.00
Published on Web 01/13/1998

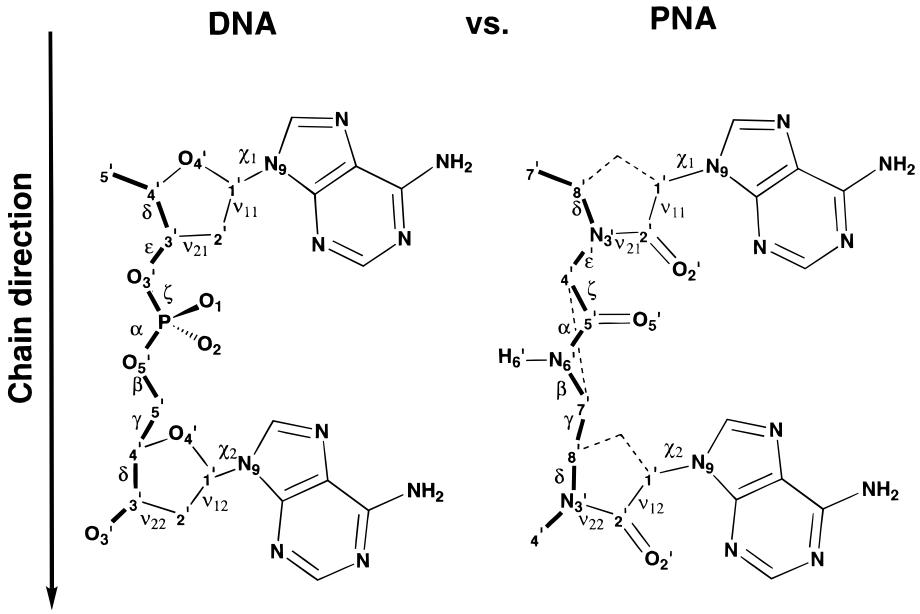

Figure 1. Internal segment of a (2-aminoethyl)glycine PNA chain backbone (right) comparing chemical bonds, backbone (in boldface), and torsion angles with a standard DNA fragment (left). Note the 1:1 replacement of DNA atoms by other atoms in PNA and the correspondence of single bond torsions—an amendment of the nomenclature introduced in a recent review of PNA structures.[45] Except for the $H_{6'}$ atom implicated in intermolecular interactions, hydrogens are not shown here. Dotted lines are introduced in PNA between $C_{1'}$ and $C_{8'}$ atoms to highlight the missing sugar ring and between $C_{4'}$ and $C_{7'}$ to emphasize the planar amide linkage.

Hoogsteen pairing with the purine strand of a 3′-5′-linked poly(dT)·poly(dA) duplex.[20]

The present study takes advantage of the methodology introduced in the preceding paper[21] to construct hybrid DNA/RNA triple helixes to treat multistranded polymer complexes with unusual chemical backbones. The repositioning of individual bases with respect to the modified chain skeletons displaces successive Watson·Crick+Hoogsteen hydrogen-bonded base pair triplets in the core of the complex. The model building thus includes the search of translational variables not considered in ref 21. The bases, however, are rearranged as a group, preserving the standard Pyr·Pu+Pyr* hydrogen-bonded base triple, rather than independently optimized to yield other modes of association (see refs 22−26 for examples of such hydrogen-bonding schemes). PNA constructs generated in this fashion correspond closely to recent crystallographic observations,[9,13] while the 2′-5′ nucleic acid complexes show reasonable agreement with currently available thermodynamic data.[17]

Methods

PNA Modeling. The commonly studied (2-aminoethyl)glycine PNA chain, illustrated in Figure 1, is conformationally much more complex than DNA. While the backbone connecting adjacent bases in the PNA corresponds in an approximate 1:1 atom-for-atom sense to the glycosyl and sugar−phosphate bonds of DNA, the replacement of the sugar ring by a linear bond sequence introduces torsional freedom not present in the nucleic acid. A total of 12 acyclic torsion angles determines the conformation of adjacent bases in PNA versus nine variables, including the sugar ring, in DNA. The increased number of ways to link a given arrangement of bases makes the search for covalent chain closure a more formidable task in PNA than in DNA. The investigation carried out here is simplified by taking advantage of the known planar geometry of the amide linkage and by restricting attention to homopolymer models. The analysis is further limited to chains with directionality mimicking that of the nucleic acid triplex, i.e., $N_{3'}\cdots C_{7'}$ virtual bonds pointed in the same sense as the $C_{3'}\cdots C_{5'}$ virtual bonds of the corresponding nucleic acid chain (see Figure 1).

The 12 torsions of PNA are divided into two groups. The first group, the independent variables, includes rotation angles (χ_1, ν_{11}, ν_{21}, ϵ, δ, ν_{22}, ν_{12}, χ_2) analogous to the glycosyl and ring torsional variables of the nucleic acid. The second set, the dependent torsions (ζ, α, β, γ), arise in the successful closure of the PNA backbone. A given set of independent angles and the assumed spatial arrangement of adjacent bases establishes the positions of the $C_{4'}$, $C_{5'}$, and $C_{7'}$ atoms (Figure 1). The resulting $C_{4'}\cdots C_{7'}$ distance, which must correspond to the standard $C^{\alpha}\cdots C^{\alpha}$ peptide virtual bond length determines chain closure. The $C_{4'}\cdots C_{7'}$ virtual bond and the $C_{4'}-C_{5'}$ bond further define the peptide plane. If the $C_{4'}\cdots C_{7'}$ distance conforms to typical (trans or cis) values, the $N_{6'}$ atom can be fixed in this plane using the characteristic amide bond length and valence angles.[27] The resulting $N_{6'}-C_{7'}$ bond length and the adjacent $C_{5'}-N_{6'}-C_{7'}$ and $N_{6'}-C_{7'}-C_{8'}$ valence angles must also fall in allowed ranges before the chain conformation is accepted. Restricting the conformational search to polymer solutions, that is to monomeric units which can be combined to form a long regularly repeating chain, further simplifies the study. This is achieved by taking $\chi_1 = \chi_2$, $\nu_{11} = \nu_{12}$, and $\nu_{21} = \nu_{22}$. The single bond torsions are varied at 10° increments over the range of 0−350°, while the peptide unit is fixed in a trans conformation with the $C_{4'}\cdots C_{7'}$ distance set at ∼3.8 Å. Because the peptide unit is a planar structure, location of the $O_{5'}$ and $H_{6'}$ PNA atoms is straightforward.

Nucleic Acid Constructs. The steps taken to form the 2′−5′ nucleic acid backbone are similar to those used in ref 21 to model ordinary DNA and RNA chains. The glycosyl and sugar torsions are treated as independent variables, with the resulting $O_{2'}\cdots O_{5'}$ distances used to

(19) Singh, R. K.; Takai, K.; Takaku, H. *Nucleic Acids Symp. Ser.* **1996**, 119−120.
(20) Lalitha, V.; Yathindra, N. *Curr. Sci.* **1995**, *68*, 68−75.
(21) Srinivasan, A. R.; Olson, W. K. **1998**, *120*, 484−491.
(22) Cheng, Y.-K.; Pettitt, B. M. *J. Am. Chem. Soc.* **1992**, *114*, 4465−4474.
(23) Piriou, J. M.; Ketterlé, C.; Gabarro-Arpa, J.; Cognet, J. A. H.; Le Bret, M. *Biophys. Chem.* **1994**, *50*, 323−343.
(24) Zhurkin, V. B.; Raghunathan, G.; Ulyanov, N. B.; Camerini-Otero, R. D.; Jernigan, R. L. *J. Mol. Biol.* **1994**, *239*, 181−200.
(25) Zhurkin, V. B.; Raghunathan, G.; Ulyanov, N. B.; Camerini-Otero, R. D.; Jernigan, R. L. In *Proceedings of the Eighth Conversation Structural Biology: The State of the Art*; Sarma, R. H., Sarma, M. H., Eds.; Adenine Press: Schenectady, NY, 1994; pp 43−66.
(26) Raghunathan, G.; Miles, T. H.; Sasisekharan, V. *Biopolymers* **1995**, *36*, 333−343.
(27) Momany, F. A.; McGurie, R. F.; Burgess, A. W.; Scheraga, H. A. *J. Phys. Chem.* **1975**, *79*, 2361−2381.

locate the intervening phosphorus atom. Successful backbone closure yields four dependent torsions (ϵ, ζ, α, β) along the $C_{3'}-C_{2'}-O_{2'}-P-O_{5'}-C_{5'}-C_{4'}$ bond sequence. When the backbone solutions are monitored, the sugar puckering (P) is varied over 20 evenly spaced pseudorotational states, and the exocyclic $C_{5'}-C_{4'}$ (γ) and glycosyl (χ) torsions over 36 evenly spaced angles between 0° and 350°. A total of 25 920 backbone combinations is tested for each arrangement of adjacent bases, a number that reflects our focus on regular polymer models made up of identical monomer units (i.e., $P_1 = P_2$, $\chi_1 = \chi_2$, where the subscript denotes residue number).

Triple Helix Formation. Triple helixes are first constructed from three independently generated 16-residue single-stranded helixes consistent with the pyrimidine·purine+pyrimidine base pairing in the canonical fiber diffraction model.[12] The intra- and intermolecular energies of the resulting complexes are assessed with the set of potential functions and constants outlined in ref 21. Intrinsic torsional contributions to rotations around the amide links of the PNA are obtained using a standard 2-fold potential with a barrier height of 10 kcal mol^{-1} for the C−C−N−C bond sequence.[27] The atoms in the peptide units are assigned partial atomic charges derived from CNDO/2 molecular orbital calculations.[28,29]

To understand the effect of base translations on the triple-helical models, we introduce limited Δx and Δy displacements of the base triples in the helical reference frame (see Figure 1 of ref 21). We generate independent polymeric backbones for all three single strands of the complex and, following our previous treatment of 3′−5′ chain units,[21] rank each set according to its total conformational energy. We determine a number of parameters which are independent of chemical connectivity (i.e., 3′−5′, PNA, or 2′−5′) and several other quantities which depend on atomic organization. The former set includes the nonbonded distances between $C_{1'}$ atoms of successive bases on the Pyr, Pu, and Hoogsteen single strands ($d_{C1'...C1'}$), the helical radii of the $C_{1'}$ atoms ($r_{C1'}$), and the angles and distances, i.e., Twist, Tilt, Roll, Shift, Slide, Rise,[30] relating the Watson−Crick (Pyr·Pu) base pairs of neighboring residues. The parameter set that depends on backbone identity contains the groove widths, backbone radii, and assorted virtual bond lengths.

Results

PNA-Linked Triplexes. A search of (2-aminoethyl)glycine PNA backbones linking successive PyrPyr, PuPu, and Pyr*Pyr* bases of the triple-stranded helix has been carried out with base triplets initially fixed in the canonical 12-fold ($\theta = 30°$) fiber reference state[12] with a per residue displacement $\Delta x\Delta y\Delta z = (0$ Å, 0 Å, 3.26 Å). The computed numbers of PNA backbones with acceptable valence angle geometry at the three different steps are far smaller than the number of possibilities considered (PyrPyr = 159, PuPu = 177, Pyr*Pyr* = 172 out of 1 679 616 total candidates for each). The allowed backbones drop precipitously (to 1, 4, and 4, respectively) when a 10 kcal mol^{-1} relative energy limit (above the lowest computed energy) is introduced at each step. Corresponding backbone structures have been sought for PNA-linked PyrPyr and Pyr*Pyr* steps and DNA-joined PuPu bases assuming a helical twist of 22.9° (15.7 residue/turn) and a rise per residue of 3.4 Å consistent with the recent crystal structure.[9] Various displacements of adjacent base triples, $\Delta x\Delta y = (0 \pm 1$ Å, 0 ± 1 Å), have also been considered. To reduce computing time, the stable DNA Pu links corresponding to the different choices of base shearing were first identified. Because there are no low energy DNA backbones between Pu bases for $\Delta x\Delta y = (0$ Å, 0 Å), (-1 Å, 0 Å), or (-1 Å, 1 Å), the related PNA linkages are not examined. Of the remaining translational combinations tested for acceptable Pyr and Pyr* PNA strand connectivities, the only stable links occur when $\Delta x\Delta y = (0$ Å, -1 Å). The latter geometry has been further tested as a feasible arrangement of neighboring base triples in the all-PNA complex by seeking the possible PNA links between the PuPu base steps.

Using the lowest energy conformation of each single-stranded dimer step, 16-residue triple-helical complexes have been generated and their total nonbonded energies have been computed. The resulting complexes where $\Delta x\Delta y\Delta z = (0$ Å, 0 Å, 3.26 Å) and $\theta = 30°$ are termed canonical triplexes, (PNA·DNA+PNA)$_{canon}$ or (PNA·PNA+PNA)$_{canon}$, whereas those constructed with $\Delta x\Delta y\Delta z = (0$ Å, -1 Å, 3.4 Å) and $\theta = 22.9°$ are called base-displaced forms, (PNA·DNA+PNA)$_{displ}$ or (PNA·PNA+PNA)$_{displ}$. Side and end views of the lowest energy conformations of these two kinds of hybrids are presented in stereo in Figure 2. The PNA-linked Pyr-containing strands are colored red in both structures, the DNA-joined Pu-bearing chains are blue, and the PNA Hoogsteen-linked backbones are green. The hole down the center of the base-displaced triplex (Figure 2, lower end view) resembles a similar feature in the crystal structure,[9] i.e., P-form triplex. The large unwinding ($\Delta\theta = -7.1°$) and base translation distort the groove geometry of the (PNA·DNA+PNA)$_{displ}$ complex compared to the canonical form. The minor groove, as measured by the perpendicular distance between ribbons of $C_{5'}\cdots C_{5'}$ virtual bonds along the (red) PNA Pyr and P···P virtual bonds along the (blue) DNA Pu chains, opens by ∼6 Å, and the major groove containing the (green) DNA Pyr* strand opens by nearly 3 Å upon base unwinding and displacement. The PNA Pyr* strand is asymmetrically positioned in both complexes, lying closer to the DNA Pu strand to which it is hydrogen bonded than to the PNA Pyr strand, e.g., $d_{Pyr*...Pu} = 6.9$ Å, $d_{Pyr...Pyr*} = 21.5$ Å in (PNA·DNA+PNA)$_{displ}$ versus $d_{Pyr*...Pu} = 7.6$ Å, $d_{Pyr...Pyr*} = 17.8$ Å in (PNA·DNA+PNA)$_{canon}$. In contrast to the canonical triplex where all three strands are roughly equidistant from the common helical axis (∼11 Å backbone radii), the Pyr-bearing PNA chain is exposed and the Hoogsteen-linked PNA strand hidden relative to the Pu-bound DNA backbone of (PNA·DNA+PNA)$_{displ}$. Note the outer (red) Pyr and inner (green) Pyr* strands in the latter structure (Figure 2, bottom), where the respective radial distances of the $C_{5'}$ peptide atoms are 13.2 and 9.9 Å. The phosphorus atoms of the (blue) Pu-bearing DNA strand, by contrast, lie 11.9 Å from the helical axis.

The total energy of the (PNA·DNA+PNA)$_{canon}$ complex, computed with the different electrostatic treatments outlined in ref 21, is notably lower than that of the (PNA·DNA+PNA)$_{displ}$ hybrid (e.g., 34.6 kcal mol^{-1} versus 52.5 kcal mol^{-1} per base triple with the Hingerty dielectric treatment[31]). The energy differences appear to reflect the compression of local backbone structure in the base-displaced triplex; the DNA P···P virtual bond distances drop to 5.8 Å in (PNA·DNA+PNA)$_{displ}$ compared to 6.8 Å in (PNA·DNA+PNA)$_{canon}$. In addition, a short (1.95 Å) contact between H5′ and O2P atoms on the DNA strand and intrinsic torsional variations contribute significantly to the computed energy difference. The observed occurrence of base displaced structures in the crystal may reflect factors not considered in the present calculations (i.e., packing effects, explicit interactions with cocrystalline molecules, etc.).

The geometries of neighboring Pyr·Pu base pairs in the computed models, determined with the CompDNA software

(28) Pople, J. A. *J. Chem. Phys.* **1966**, *44*, 3289−3296.
(29) Yan, J. F.; Momany, F. A.; Hoffmann, R.; Scheraga, H. A. *J. Phys. Chem.* **1970**, *74*, 420−433.
(30) Dickerson, R. E.; Bansal, M.; Calladine, C. R.; Diekmann, S.; Hunter, W. N.; Kennard, O.; von Kitzing, E.; Lavery, R.; Nelson, H. C. M.; Olson, W. K.; Saenger, W.; Shakked, Z.; Sklenar, H.; Soumpasis, D. M.; Tung, C.-S.; Wang, A. H.-J.; Zhurkin, V. B. *J. Mol. Biol.* **1989**, *208*, 787−791.
(31) Hingerty, B. E.; Ritchie, R. H.; Ferrel, T. L.; Turner, J. E. *Biopolymers* **1985**, *24*, 427−439.

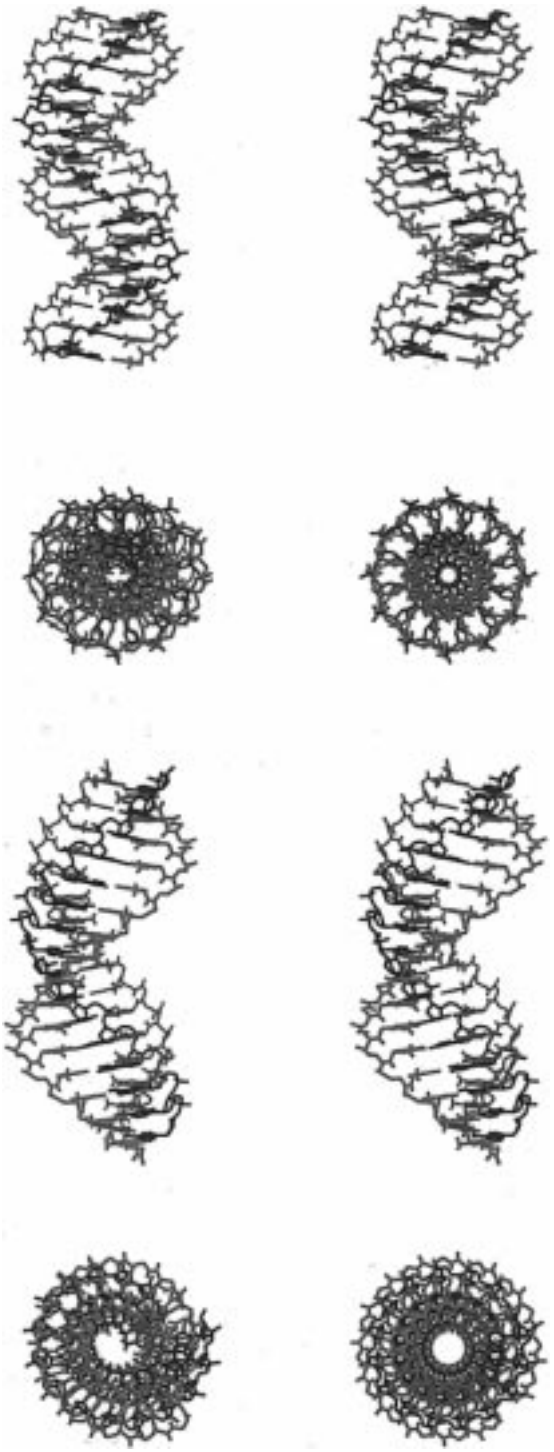

Figure 2. Side and end views, in stereo, of $(PNA{\cdot}DNA{+}PNA)_{canon}$ (top) and $(PNA{\cdot}DNA{+}PNA)_{displ}$ (bottom) hybrid triplexes. The pyrimidine-containing PNA, purine-bearing DNA, and Hoogsteen-linked PNA strands are colored in red, blue, and green, respectively.

package,[32] are compared in Table 1 against the mean values in relevant crystal structures. As expected from the choice of global helical parameters, the arrangement of successive Watson−Crick base pairs in the $(PNA{\cdot}DNA{+}PNA)_{displ}$ triplex is much closer to that in the PNA(CTCTTCTTC)·d(GAGAAGAAG)+PNA(CTCTTCTTC) hybrid crystal structure[9] than is the positioning in the canonical model. The base-displaced triplex also bears close resemblance to the observed geometry of the PNA(CGTACG)·PNA(CGTACG) duplex.[13] The scatter plots of Slide, Roll, and Twist values in Figure 3 reveal the very different local character of the canonical and translated models. The $(PNA{\cdot}DNA{+}PNA)_{displ}$ model overlaps some highly unwound forms of crystalline A-DNA, whereas the $(PNA{\cdot}DNA{+}PNA)_{canon}$ structure lies at the border between A- and B-form structures taken from the Nucleic Acid Database.[33] These data suggest how the replacement of two charged sugar−phosphate backbones in the classical triplex by PNA linkages may bring about lateral slippage of neighboring base triples in the hybrid.

The hydrogen bonding between the amide proton in the PNA Pyr* strand, i.e., $H_{6'}$ in Figure 1, and a phosphate oxygen in the nearby Pu DNA is a unique characteristic of the P-form triplex.[9] This distance, of the order of 10.5 Å in the $(PNA{\cdot}DNA{+}PNA)_{canon}$ model, drops to ∼4.3 Å in the $(PNA{\cdot}DNA{+}PNA)_{displ}$ structure. Visual inspection of the side view of the base-displaced triple-helical model (Figure 2) reveals the close association between (blue) DNA Pu and (green) PNA Pyr* backbones. This distance further drops when additional $\Delta x\Delta y$ displacements are introduced.

It should be noted that PNA strands are connected by a six-residue peptide tether in the crystal complex. The backbone conformations of the two hexapeptides linking the PNA backbones in the PNA·DNA+PNA single-crystal structure are quite different with some of the ϕ ψ torsions found in completely different ranges. The $C^{\alpha}\cdots C^{\alpha}$ end-to-end distances of the peptide linkers, however, are comparable (∼14 Å), suggesting that the peptide tethers may have little influence on the conformation of the triplex. It is also well-known from the analysis of single-crystal protein structures[34] that homologous sequences adopt similar core structures which are insensitive to the lengths and sequences of loop regions (some of which are comparable in size to the hexapeptide linker in the PNA·DNA+PNA complex).

The backbones of the triplex models are compared in Table 2 against the torsion angle ranges observed in the single-crystal PNA hybrid,[9] the standard conformations of the amide links in polypeptides,[35] and the angular values of A- and B-DNA crystal structures.[36] The energy-optimized PNA linkages adopt conformational states typical of residues in left-handed α-helixes or β-sheets (right-handed α-helical states are notably missing). The nonpeptide backbone, however, does produce these secondary structures. The computed data are, nevertheless, in good agreement with the observed torsions in the hybrid crystal.[9] As might be expected from the choice of modeling conditions, the PNA strands of the base-displaced triplex correspond more closely to the experimental backbones than do those of the canonical model. Neither model matches the DNA backbone of the crystalline hybrid triplex, which has a mixture of A- and B-like features. The lack of correspondence between nucleic acid torsion angles, however, is not always indicative of structural dissimilarity. Large correlated variations in selected nucleic acid torsions can preserve overall polymeric features,[37,38]

(32) Gorin, A. A.; Zhurkin, V. B.; Olson, W. K. *J. Mol. Biol.* **1995**, *247*, 34−48.

(33) Berman, H. M.; Olson, W. K.; Beveridge, D. L.; Westbrook, J.; Gelbin, A.; Demeny, T.; Hsieh, S.-H.; Srinivasan, A. R.; Schneider, B. *Biophys. J.* **1992**, *63*, 751−759.

(34) Thornton, J. M. *Nature* **1990**, *343*, 411−412.

(35) Kendrew, J. C.; Klyne, W.; Lifson, S.; Miyazawa, T.; Némethy, G.; Phillips, D. C.; Ramachandran, G. N.; Scheraga, H. A. *Biochemistry* **1970**, *9*, 3471−3479.

(36) Schneider, B.; Neidle, S.; Berman, H. M. *Biopolymers* **1997**, *42*, 113−124.

(37) Olson, W. K. In *Biomolecular Stereodynamics*; Sarma, R. H., Ed.; Adenine Press: New York, 1981; pp 327−343.

Table 1. Comparative Base Geometry of PNA·DNA+PNA Triple-Helical Models and Related Crystal Structures

Twist (deg)	Tilt (deg)	Roll (deg)	Shift (Å)	Slide (Å)	Rise (Å)	structure
29.5	−2.2	4.9	0.0	−1.1	3.5	$(PNA{\cdot}DNA{+}PNA)_{canon}$
22.5	−1.7	3.8	−0.2	−1.7	3.7	$(PNA{\cdot}DNA{+}PNA)_{displ}$
$22.1_{\pm1.7}$	$0.2_{\pm2.5}$	$3.0_{\pm2.5}$	$1.0_{\pm0.2}$	$-2.3_{\pm0.1}$	$3.3_{\pm0.1}$	PNA(CTCTTCTTC)·d(GAGAAGAAG)+PNA(CTCTTCTTC)[a]
$19.9_{\pm2.1}$	$-0.5_{\pm1.3}$	$3.1_{\pm4.7}$	$0.0_{\pm0.2}$	$-2.5_{\pm0.5}$	$3.4_{\pm0.3}$	PNA(CGTACG)·PNA(CGTACG)[b]
$31.0_{\pm4.4}$	$0.0_{\pm3.1}$	$7.5_{\pm5.1}$	$0.0_{\pm0.5}$	$-1.6_{\pm0.4}$	$3.3_{\pm0.3}$	370 A-DNA steps in 34 crystal structures[c]
$35.9_{\pm5.9}$	$0.0_{\pm3.2}$	$0.2_{\pm5.4}$	$0.0_{\pm0.5}$	$0.2_{\pm0.8}$	$3.3_{\pm0.2}$	484 B-DNA steps in 44 crystal structures[d]

[a] Reference 9. [b] Reference 13. [c] Nucleic Acid Database[33] structures: addb01, adh006, adh007, adh008, adh010, adh012, adh014, adh020, adh023, adh024, adh026, adh027, adh030, adh031, adh038, adh041, adh056, adh057, adh058, adh059, adj022, adj049, adj050, adj051, adl025, adl045, adl046, ahj015, ahj040, ahj043, ahj044, ahj052, ahj060, ahjs55. [d] Nucleic Acid Database[33] structures: bdj008, bdj017, bdj019, bdj031, bdj036, bdj037, bdj039, bdj051, bdj052, bdj055, bdj060, bdjb27, bdjb43, bdjb44, bdjb48, bdjb57, bdl005, bdl006, bdl007, bdl009, bdl011, bdl012, bdl014, bdl015, bdl022, bdl028, bdl029, bdl038, bdl042, bdl046, bdl047, bdl059, bdlb03, bdlb04, bdlb10, bdlb13, bdlb26, bdlb33, bdlb40, bdlb41, bdlb53, bdlb54, bdlb56.

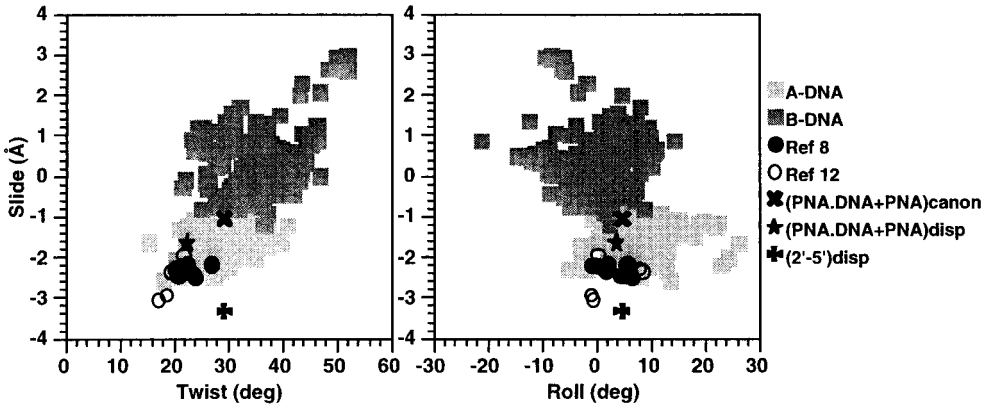

Figure 3. Comparative plot of Twist, Roll, and Slide parameters characterizing the geometry of successive Watson−Crick base pairs in the $(PNA{\cdot}DNA{+}PNA)_{canon}$ and $(PNA{\cdot}DNA{+}PNA)_{displ}$ hybrid triplex models with individual dimer steps in related single-crystal structures.

Table 2. Torsion Angle Ranges of PNA(Pyr)·d(Pu)+PNA(Pyr*) and PNA(Pyr)·PNA(Pu)+PNA(Pyr*) Repeating Units in Low-Energy Triplex Models and X-ray Crystal Structures[a]

base	PNA model	χ_1	ν_{11}	ν_{21}	ϵ	ζ	α	β	γ	δ	ref
Pyr	$(PNA)_{canon}$	g^+	t	g^-	g^+	g^+	t	s^+	g^+	g^+	
Pyr	$(PNA)_{displ}$	g^-	t	t	g^+	s^+	t	t	g^+	g^+	
Pyr	$(PNA)_{cryst}$	g^-	t	t	g^+	c	t	s^-	g^+	g^-	9
Pyr*	$(PNA)_{canon}$	g^+	s^-	c	s^+	t	t	g^+	g^+	g^+	
Pyr*	$(PNA)_{displ}$	g^-	t	t	g^+	c	t	s^-	g^+	g^+	
Pyr*	$(PNA)_{cryst}$	g^-	t	t	g^+	c	t	s^-	g^+	g^-	9
Pu	$(PNA)_{canon}$	g^+	t	g^-	g^+	s^+	t	s^+	g^+	g^+	
Pu	$(PNA)_{displ}$	g^-	t	t	g^+	t	t	g^+	g^+	g^+	
	polypeptide		ψ	ω	ϕ	ψ	ω	ϕ			ref
	RH-α-helix		g^-	t	g^-	g^-	t	g^-			35
	LH-α-helix		g^+	t	g^+	g^+	t	g^+			35
	β-strand		s^+	t	s^-	s^+	t	s^-			35
base	nucleic acid model	χ	ν_{11}	ν_{21}	ϵ	ζ	α	β	γ	δ	ref
Pu	$(DNA)_{canon}$	g^-	t	g^+	t	g^-	s^-	g^+	t	s^+	
Pu	$(DNA)_{displ}$	s^-	g^+	t	s^-	g^+	g^+	g^-	t	g^+	
Pu	$(DNA)_{cryst}$	s^-	g^+	t	t	g^-	g^-	t	g^+	g^+	9
	A-DNA	s^-	g^+	t	t	g^-	g^-/t	t	g^+/t	g^+	36
	B-DNA	g^-	t	g^+	t/g^-	g^-/t	g^-	t	g^+	t	36

[a] See Figure 1 for the bond sequences defining torsions, α-ζ in terms of the backbone highlighted in boldface, χ by $C_8{-}N_9{-}C_{1'}{-}C_{2'}$, ν_{11} in terms of $N_9{-}C_{1'}{-}C_{2'}{-}C_{3'}$ (DNA) or $N_9{-}C_{1'}{-}C_{2'}{-}N_{3'}$ (PNA), and ν_{21} as $C_{1'}{-}C_{2'}{-}C_{3'}{-}O_{3'}$ (DNA) or $C_{1'}{-}C_{2'}{-}N_{3'}{-}C_{4'}$ (PNA). Angles classified as cis ($c = 0° \pm 20°$), gauche$^\pm$ ($g^\pm = \pm60° \pm 40°$), skew$^\pm$ ($s^\pm = \pm120° \pm 20°$), or trans ($t = 180° \pm 40°$).

whereas small changes in other angles can have dramatic effects on global structure.[39,40]

The backbone torsions corresponding to Pu-linked PNA strands in canonical and base-displaced configurations are also reported in Table 2. Triple helixes made up exclusively of PNA chains look very similar to the corresponding hybrid structures shown in Figure 2 (atomic coordinates of these and all other models described herein are available upon request from the authors; see also the Supporting Information). Our preliminary computations, however, do not distinguish any energetic preferences for either of these all-PNA models; the canonical positioning of base triplets reduces the total energy per base triple of the $(PNA{\cdot}PNA{+}PNA)_{displ}$ model computed by the Hingerty dielectric treatment[31] by only 3 kcal mol^{-1}. The rearrangement also has limited effect on the computed numbers of low-energy solutions (16 for canonical verses 8 for base-

(38) Srinivasan, A. R.; Olson, W. K. *J. Biomol. Struct. Dyn.* **1987**, *4*, 895−938.
(39) Olson, W. K. *Biopolymers* **1976**, *15*, 859−878.
(40) Yathindra, N.; Sundaralingam, M. *Nucleic Acids Res.* **1976**, *3*, 729−747.

Table 3. Number of Pyrimidine (Pyr), Purine (Pu), and Hoogsteen (Pyr*) Polymer Building Blocks with 2′−5′ (boldface) and 3′−5′ Backbone Linkages Corresponding to Different $\Delta x\Delta y$ Shearing in the Helical Reference Frame

	Δy(Å)		
Δx(Å)	−2	0	2
	Acceptable Valence Angle Connections		
−2	**43**, **33**, **4**	**121**, **15**, **30**	**87**, **3**, **105**
	0, 35, 23	68, 43, 83	156, 29, 139
0	**159**, **120**, **16**	**53**, **74**, **64**	**23**, **48**, **95**
	0, 3, 142	160, 139, 150	66, 233, 43
2	**90**, **11**, **88**	**20**, **120**, **155**	**1**, **123**, **28**
	0, 0, 142	146, 0, 0	28, 44, 0
	Low-Energy Forms[a]		
−2	**1**, **1**, **1**	**1**, **1**, **1**	**2**, **1**, **1**
	0, 11, 1	2, 1, 3	1, 1, 1
0	**6**, **8**, **1**	**4**, **4**, **1**	**1**, **2**, **3**
	0, 3, 1	7, 14, 13	1, 1, 1
2	**6**, **1**, **5**	**1**, **8**, **14**	**1**, **1**, **1**
	0, 0, 1	2, 0, 0	1, 3, 0

[a] Number of backbone solutions within 10 kcal mol^{-1} of the lowest energy connection between designated bases under the given conditions.

Table 4. Helical Radii (in boldface) and Virtual Bond Distances of Successive $C_{1'}$ Atoms in Pyrimidine (Pyr), Purine (Pu), and Hoogsteen (Pyr*) Strands of Regular 2′−5′-Linked Triplexes Corresponding to Different $\Delta x\Delta y$ Shearing in the Helical Reference Frame

	Δy(Å)		
Δx(Å)	−2	0	2
−2	**13.1**, **8.8**, **3.2**	**10.2**, **5.3**, **5.1**	**8.1**, **2.7**, **8.4**
	7.5, 5.6, 3.7	6.2, 4.2, 4.2	5.3, 3.5, 5.4
0	**11.3**, **10.6**, **7.1**	**7.8**, **7.9**, **8.1**	**4.7**, **6.5**, **10.5**
	6.7, 6.4, 4.9	5.2, 5.2, 5.3	4.1, 4.7, 6.3
2	**10.8**, **13.3**, **11.0**	**6.9**, **11.3**, **11.7**	**3.1**, **10.3**, **13.4**
	6.5, 7.6, 6.6	4.8, 6.7, 6.9	3.6, 6.3, 7.7

displaced). Further studies are needed to gain a better understanding of all-PNA triplex formation and of 1:2 PNA:DNA triplexes (e.g., DNA·DNA+PNA, DNA·PNA+DNA, etc.). For example, the PNA linkages of purine bases in the canonical and base-displaced forms have not been fully explored. Initial attempts to model DNA·DNA+PNA with triplex in base displaced and canonical geometries yield comparative numbers of low-energy backbones, but almost all solutions have unusual $O_{1'}$-endo sugar puckers in the DNA.

2′−5′ Triple Helixes. The numbers of 2′-5′ sugar−phosphate links found in the Pyr, Pu, and Pyr* strands of regular 12-fold ($\theta = 30°$) triple helixes are presented (in boldface) in Table 3. While many single-stranded structures with acceptable valence angle geometries can be generated for the different base arrangements, $\Delta x\Delta y\Delta z$ = (0 ± 2 Å, 0 ± 2 Å, 3.26 Å), only two combinations lead to energetically acceptable 2′−5′-linked triplexes. Complex formation corresponding to $\Delta x\Delta y$ combinations of (−2 Å, ±2 Å), (0 Å, ±2 Å), (2 Å, 2 Å), and (±2 Å, 0 Å) is ruled out by the lack of backbone connections at some steps (Table 3, upper half) or the absence of low-energy conformations in others (Table 3, lower half). Most of the energetic restrictions stem from the close separation of adjacent bases along the 2′-5′ strands (evident from the very short $C_{1'}\cdots C_{1'}$ virtual bond distances, $d_{C1'\cdots C1'}$, and small atomic radii, $r_{C1'}$, in Table 4). These restrictions similarly rule out 3′−5′-linked triplexes (described in Table 3 by the numerical values in plain font). Indeed, the only acceptable (low-energy) 3′−5′ triplex occurs when the base triples are positioned in the standard helical reference state, $\Delta x\Delta y$ = (0 Å, 0 Å). Subsequent analyses are thus restricted to 3′−5′-linked triplexes in the canonical frame, here termed $(3'-5')_{canon}$, and 2′−5′-linked triple helixes with bases in the canonical and $\Delta x\Delta y$ = (2 Å, −2 Å) base-displaced forms, respectively labeled $(2'-5')_{canon}$ and $(2'-5')_{displ}$.

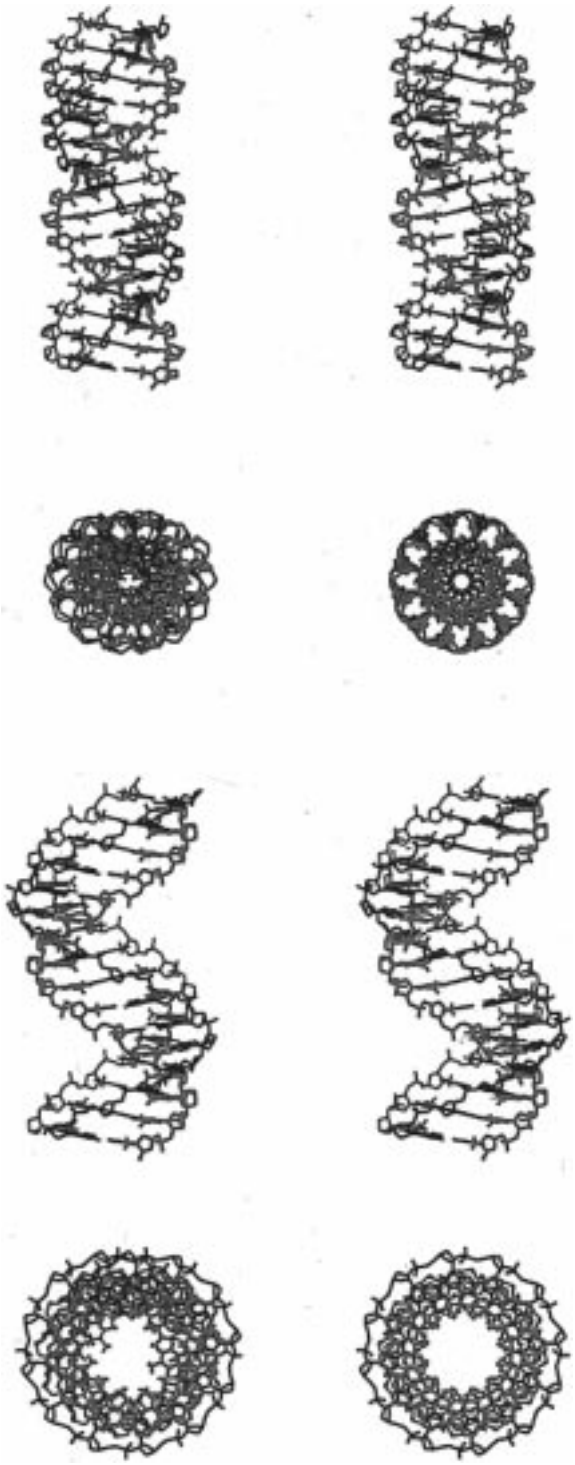

Figure 4. Side and end views, in stereo, of the lowest energy $(2'-5')_{canon}$ (top) and $(2'-5')_{displ}$ (bottom) triple helixes Pyr, Pu, and Pyr*. Strands are color-coded as in Figure 2.

Side and end views of two low-energy 2′−5′-linked $(T\cdot A+T)_{16}$ triplexes, one corresponding to the canonical and the other to the base-displaced form, are shown in Figure 4. The sugars in the three strands of both complexes adopt $C_{2'}$-endo puckering. Nonbonded energies computed on the basis of the electrostatic treatments outlined in ref 21 consistently favor the $(2'-5')_{displ}$ structure over the $(2'-5')_{canon}$ form. The end views of the two complexes (Figure 4) reveal the increased diameter of the base-

displaced triplex, with a wide hole through its center, compared to the canonical structure. This chain extension apparently accounts for the energetic differences. The overall similarity of these structures with the corresponding PNA complexes is striking (compare Figures 2 and 4). As in PNA, the shearing of base triples perturbs the groove structure of the 2′−5′ triplex, but unlike PNA, where the minor groove opens upon base displacement, the minor groove (between red and blue strands) is narrowed in $(2'-5')_{displ}$ compared to $(2'-5')_{canon}$. The 2′−5′ major groove, however, mimics PNA in widening (from 17.9 to 24.5 Å) with base translation and in positioning the (green) Pyr* strand close to the (blue) Pu strand. Like PNA, the three strands of the $(2'-5')_{displ}$ open disproportionately, but here the Pu strand is significantly more exposed than the Pyr and Pyr* chains ($r_{Pu} \approx 14$ Å versus backbone radii of ∼10 Å for the Pyr and Pyr* strands). The distances between neighboring phosphate groups are also greater in the translated 2′−5′ triplex than in $(2'-5')_{canon}$ ($d_{P...P}$ respectively 6.2−8.0 Å versus ∼5.7 Å).

There are no solved crystal structures of 2′−5′-linked nucleic acid triplexes. The best available experimental model is the NOE-refined 2′−5′-linked duplex, 5′-CGGCGCCG-2′,[41] characterized by a −4.2 Å Δ*x*-shear displacement and a 21° inclination of Watson−Crick base pairs with respect to the global helical axis. Base inclination is generally tied to significant changes in the roll angle,[42] a parameter not explicitly included in this work. The NMR data also reveal a mixed sugar puckering along the chain backbone with the pseudorotation phase angle ranging between 20° ($C_{3'}$-endo) and 228° ($C_{2'}$-endo). Base pair translations and sugar repuckerings have long been known to be important factors in the formation of 2′−5′ polymer duplexes.[43] While mixed puckering is excluded from the present models, detailed searches of individual dimer steps reveal all possible combinations of $C_{3'}$-endo and $C_{2'}$-endo puckering in the low-energy linkages of Pyr, Pu, and Pyr* strands (data not shown). Thus, it should be possible to construct 2′−5′ triple-helical models with mixed sugar puckering.

As an initial step in estimating the relative stabilities of 2′−5′- and 3′−5′-linked triplexes, we have computed the electrostatic interactions between phosphate groups in a wide variety of three-stranded models. In addition to the low-energy structure illustrated in Figure 4, we have examined the interactions of charged phosphate groups (each bearing −0.152 esu) in complexes generated from all other combinations of low-energy chain backbones (i.e., Pyr, Pu, and Pyr* monomer repeating units within 10 kcal mol^{-1} of the lowest energy forms). For example, a total of 16 canonical 2′−5′ triplexes have been constructed from the 4 Pyr × 4 Pu × 1 Pyr* states listed in the lower half of Table 3 and 30 different 2′−5′ complexes with bases displaced by $\Delta x\Delta y$ = (2 Å, −2 Å). The 3′−5′-linked complexes include all possible combinations of the canonical D·D+D, D·D+R, D·R+D, D·R+R, R·R+R, R·R+D, R·D+R, and R·D+D repeating units listed in Table 2 of ref 21, leading to a total of 8680 models. Despite the variation in groove structure that accompanies the different sugar conformations, the electrostatic energies of the $(2'-5')_{displ}$ triplexes are slightly lower on average than those of the $(3'-5')_{canon}$ complexes (with respective mean values of 6.0 and 6.3 kcal mol^{-1}). The $(2'-5')_{canon}$ structures, however, are consistently high in energy (7.0 kcal mol^{-1}). The lower energy of the base-displaced form may account, at least in part, for the observed stability of 2′−5′-linked triplexes over 3′−5′-linked ones.[17]

We have additionally determined the electrostatic energies of a number of hybrid triple helixes comprised of a single 2′−5′ chain and two 3′−5′-linked strands using all combinations of the low-energy polymer building blocks. Interestingly, the computed energies are independent of the location of the 2′−5′ chain and the chemical nature of the 3′−5′ chain. For example, the mean energies of the models, based on the Hingerty dielectric treatment,[31] fall in a narrow range between 6.3 and 6.7 kcal/mol, suggestive of similar enthalpic contributions in the different hybrids. The assumed positions of base triples, however, appear to influence the location of the 2′−5′ strand within the multistranded complex (i.e., the modified backbone fits more easily in the Watson−Crick pyrimidine site than in the Hoogsteen location in both canonical and base-displaced arrangements; see Table 3) and may be related to the preferential replacement of the normal 3′−5′ pyrimidine strand by other DNA mimics.[44] The large number of conformationally acceptable solutions reveals a decided preference for the 2′−5′ phosphodiester to link the Pyr bases. For example, there are 728 low-energy $(2'-5'\cdot D+D)_{canon}$ models versus 364 for $(D\cdot 2'-5'+D)_{canon}$ and 98 for $(D\cdot D+2'-5')_{canon}$. Similarly, there are 476 $(2'-5'\cdot R+R)_{canon}$ combinations versus 196 and 119 for $(R\cdot 2'-5'+R)_{canon}$ and $(R\cdot R+2'-5')_{canon}$, respectively. The larger number of DNA versus RNA hybrid structures (1190 compared to 791) presumably reflect the close resemblance of the canonical parameters to the B-form double helix. The observed formation of thermally stable hybrids of 2′−5′-linked single strands with duplex RNA but not with DNA,[19] on the other hand, suggests that the hybrid might conform more closely to the A-form structure characteristic of RNA. Further research is needed to gain a better understanding of the relative stabilities of hybrid triple helixes containing 2′−5′-linked single strands.

Discussion

The triple-helical models generated in this study provide new hints of essential features in a good DNA mimic. While multistranded complex formation calls for base side groups that can adopt the requisite Watson−Crick and Hoogsteen pairings, a well-designed chemical replacement must also conform to the preferred arrangements of the sugar−phosphate backbone. The elimination of the sugar ring and replacement of the phosphate by an amide in PNA, for example, introduce rotational flexibility that presumably allows the modified chain to respond to the conformational dictates of the nucleic acid.[45] Our survey of three-dimensional hybrid structures, however, indicates that the chemical features of PNA contribute substantially to global features of the molecular complex. Specifically, the replacement of DNA by PNA distorts the canonical triple helix, displacing the hydrogen-bonded bases away from the global helical axis. The base pair parameters (Figure 3) and individual torsion angles (Table 2) in simulated and experimentally characterized PNA·DNA+PNA complexes are diagnostic of an extreme A-type structure. The canonical DNA triplex, by contrast, is a structure intermediate between the A- and B-form helixes in terms of base positioning and chain conformation.

As is well-known,[46] the sugar puckering is one of several conformational features that distinguish A-DNA from B-DNA.

(41) Robinson, H.; Jung, K.-E.; Switzer, C.; Wang, A. H. *J. Am. Chem. Soc.* **1995**, *117*, 837−838.
(42) Calladine, C. R.; Drew, H. R. *J. Mol. Biol.* **1984**, *178*, 773−782.
(43) Srinivasan, A. R.; Olson, W. K. *Nucleic Acids Res.* **1986**, *14*, 5461−5479.
(44) Nielsen, P. E.; Egholm, M.; Berg, R. H.; Buchardt, O. *Science* **1991**, *254*, 1497−1500.
(45) Eriksson, M.; Nielsen, P. E. *Quart. Rev. Biophys.* **1996**, *29*, 369−394.
(46) Saenger, W. *Principles of Nucleic Acid Structure*; Springer-Verlag: New York, 1984; Chapter 11.

The standard descriptors of ring geometry—internal ring torsions and phase angle of pseudorotation,[47] out-of-plane atomic displacements,[48] etc.—however, ignore parameters such as ν_{11} and ν_{21} (Figure 1) that relate base and backbone atoms. The planar $C_{2'}-N_{3'}$ linker of the PNA amide side group simulates the trans arrangement ν_{21} in the A-DNA helix, but precludes formation of the g^+ conformer typical of B-DNA (Table 2). The tendency of PNA to adopt A-like helical structures is therefore expected. The $C_{2'}$-endo sugar puckering characteristic of the B-form helix, by contrast, places the glycosyl and $C_{2'}-C_{3'}$ bonds in a trans conformation of ν_{11}. Alternative chemistries which might be considered to fix a PNA-like structure in the B-form by a double bond, however, are unrealistic (since the replacement of $C_{1'}$ by an sp^2 center would make the glycosyl bond chemically labile). Thus, PNA is inconsistent with the B-form, and the design of B-like analogues necessitates a different chemical approach.

The placement of the peptide linkage along the PNA backbone also influences global helical structure. Perturbations of the phosphodiester torsions from the *gauche*$^-$ arrangements found in A- and B-type nucleic acid helixes typically unwind, bend, and/or displace the flanking base pair steps.[49] The replacement of either phosphodiester torsion by a planar double bond tends to distort the B-form helix. While correlated changes in other backbone angles may sometimes counter these deformations,[37] a design that substitutes rigid chemical linkers for naturally extended backbone bonds should help to foster canonical helical torsions. For example, the inversion of the (2-aminoethyl)glycine PNA backbone (with respect to the N_6-H_6' bond in Figure 1) moves the amide linkage to atomic locations normally folded in a trans conformation (i.e., the $P-O_{5'}-C_{5'}-C_{4'}$ bond sequence in the nucleic acid). Preliminary computational analysis of this so-called parallel orientation of PNA[50] reveals low-energy backbone linkages between Pyr and Pyr* bases in the canonical triple helix geometry. One such dimer step is compared with a base displaced arrangement of the antiparallel PNA backbone in Figure 5. As pointed out above, the antiparallel strand closes more successfully when the base triple is displaced from the helical axis. The accompanying changes in base geometry between the two dimer models may underlie the characteristic circular dichroism spectra of parallel and antiparallel PNA·DNA oligomer complexes.[50]

The computed slippage of bases in the 2′−5′ nucleic acid triplex, while globally similar to that found in the PNA·DNA+PNA hybrid, reflects a very different chemical driving force. The side group between the base and backbone shortens with the rearrangement which incorporates the $C_{2'}-C_{3'}$ bond in the chain backbone. The strong intrinsic conformational preferences of the sugar ring and phosphodiester apparently drive the base repositioning. Base slippages and unwinding of the sort found in PNA and 2′−5′ triplex models occur as well at recognition sites in single-crystal structures of duplex DNA bound to various proteins.[51] Chemical analogues which induce comparable restructuring of DNA could thus prove useful in dissecting the relative contributions of base and backbone to the nucleic acid recognition process.

The conformational principles gleaned from this work also help make sense of other nucleic acid mimics. The binding affinity of antisense agents presumably reflects their ability to form A-type helixes with RNA targets. Molecules which introduce appropriate double bonds in the side group (i.e., ν_{21}) and/or replace the natural phosphodiester linkage in DNA by rigid links help lock the bases in the requisite (unwound and laterally sheared) geometry. Selected amide modifications of the phosphodiester, for example, yield strands with higher affinity toward an RNA target than the corresponding DNA complement with ΔT_m increases up to 0.4° per modification.[52] The combined variation of backbone and side chain in PNA adds further stabilization with ΔT_m rising well over 1° per modified unit in both PNA·RNA and PNA·DNA complexes.[45] While antigene molecules, in principle, can form either A- or B-type complexes with their DNA targets, PNA and 2′−5′ linked molecules clearly associate with DNA as extreme A-like hybrids. The natural restrictions of these complexes to a single conformational domain add to the electrostatic and hydrogen-bonding contributions that stabilize these triplexes. The design of stable B-like hybrids can build upon principles learned from the combined analysis of nucleic acid base and backbone structure.

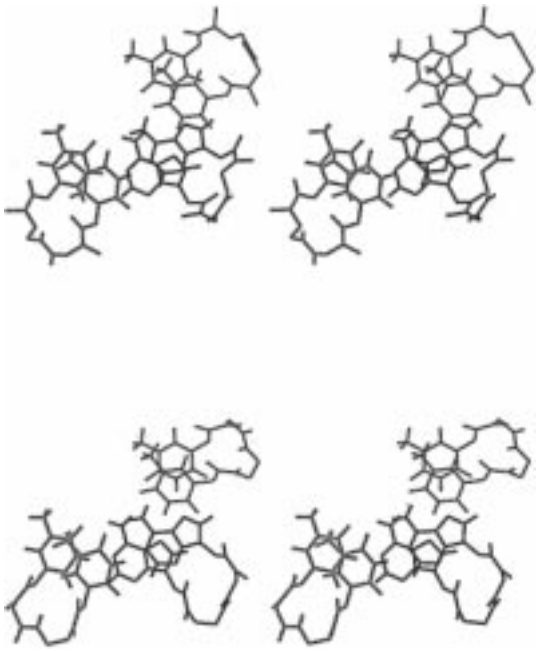

Figure 5. Comparative stereo images of parallel and antiparallel T·A+T dimer steps respectively in canonical (top) and base-displaced (bottom) triple helix arrangements. Strands are color-coded as in Figure 2.

Acknowledgment. Sponsorship of this research by the U.S. Public Health Service under research grant GM-20861 is gratefully acknowledged. We are also grateful to Drs. L. Betts and S. Jordan for sharing X-ray and NMR data on PNA/DNA triple- and double-helical complexes and to Dr. G. L. Olson for discussions of chemical structure and reactivity. Computations were performed at the Rutgers Center for Computational Chemistry. Stereo images were generated with a PostScript graphics program developed in this laboratory.

Supporting Information Available: Tables of atomic coordinates for Figures 2, 4, and 5 (98 pages). See any current masthead page for ordering information and Web access instructions.

(47) Altona, C.; Sundaralingam, M. *J. Am. Chem. Soc.* **1972**, *94*, 8205−8212.
(48) Cremer, D.; Pople, J. A. *J. Am. Chem. Soc.* **1975**, *97*, 1354−1358.
(49) Taylor, E. R.; Olson, W. K. *Biopolymers* **1983**, *22*, 2667−2702.
(50) Egholm, M.; Buchardt, O.; Christensen, L.; Behrens, C.; Freier, S. M.; Driver, D. A.; Berg, R. H.; Kim, S. K.; Norden, B.; Nielsen, P. E. *Nature (London)* **1993**, *365*, 566−568.
(51) Olson, W. K. *Curr. Opin. Struct. Biol.* **1996**, *6*, 242−256.
(52) Wolf, R. M.; Mesmaeker, A. D.; Waldner, A.; Wendeborn, S.; Fritsch, V.; Lebreton, J. *New J. Chem.* **1997**, *21*, 61−72.